Journal of Materials Chemistry A

ROYAL SOCIETY OF CHEMISTRY

PAPER

View Article Online
View Journal | View Issue

Cite this: J. Mater. Chem. A, 2022, 10, 13492

Achieving 15.81% and 15.29% efficiency of all-polymer solar cells based on layer-by-layer and bulk heterojunction structures†

Wenjing Xu,[a] Xixiang Zhu,[a] Xiaoling Ma,*[a] Hang Zhou,[b] Xiong Li,[c] Sang Young Jeong,[d] Han Young Woo,[d] Zhengji Zhou,*[e] Qianqian Sun*[b] and Fujun Zhang*[a]

Received 11th April 2022
Accepted 6th June 2022

DOI: 10.1039/d2ta02914f

rsc.li/materials-a

Wide bandgap polymer donor PM6 and narrow bandgap polymer acceptor PY-IT were selected to construct all-polymer solar cells (all-PSCs) with a layer-by-layer (LbL) or bulk heterojunction (BHJ) structure. The solvent additive 1-chloronaphthalene (CN) plays a vital role in improving the performance of all-PSCs. The power conversion efficiency (PCE) of LbL all-PSCs is improved to 15.81% from 13.67% by incorporating 1 vol% CN in PY-IT solution, benefiting from the simultaneously enhanced short circuit current density (J_{SC}) of 22.61 mA cm^{-2} and fill factor (FF) of 73.62%. A similar phenomenon is also observed in BHJ all-PSCs whose PCE increased from 13.29% to 15.29% by incorporating 1 vol% CN in PM6:PY-IT blend solution, originating from the optimized phase separation for better exciton dissociation and charge transport in the BHJ active layers. Over 15% PCE improvement can be obtained in the BHJ and LbL all-PSCs by incorporating appropriate additive CN as a morphology regulator. It should be noticed that the PCEs of LbL all-PSCs with CN are higher than those of other all-PSCs, indicating that the LbL processing method combined with the additive should be a prospective strategy to fabricate highly efficient all-PSCs.

Introduction

All-polymer solar cells (all-PSCs) consisting of polymer donors and polymer acceptors have attracted extensive attention due to their superior features such as excellent mechanical durability and stability, as well as an outstanding film-forming property for large area roll-to-roll manufacturing. Benefiting from material innovation and device engineering, over 15% power conversion efficiency (PCE) of all-PSCs has been achieved in several studies.[1–4] However, it should be noticed that the evolution of all-PSCs still lag behind that of small molecule acceptor based PSCs with PCEs over 19%, which is mainly due to the morphology regulation difficulty of active layers in commonly employed bulk heterojunction (BHJ) all-PSCs.[5–8] The active layer morphology optimization is a huge challenge in BHJ all-PSCs because neighboring polymer chains are strongly intertwined and entangled during one step spin-coating of the polymer mixture solution. Very recently, the layer-by-layer (LbL) processing method has attracted extensive attention, in which the donor and acceptor layers are sequentially cast, which is conducive to maintaining the high purity of the donor/acceptor domain for efficient charge transport in LbL active layers.[9–11] The key photovoltaic parameters of the typical studies of BHJ and LbL all-PSCs are listed in Table 1. The LbL all-PSCs exhibit a relatively large PCE in comparison with the corresponding BHJ all-PSCs prepared with the same donor and acceptor materials, suggesting that the LbL processing method may have great potential in achieving highly efficient all-PSCs. Recently, solvent additives have been separately introduced into donor or acceptor solutions to optimize the molecular arrangement and crystallites of each layer, which should be a simple and convenient strategy to further improve the performance of LbL-PSCs.[12–15] An appropriate solvent additive can play a key role in optimizing phase separation for efficient exciton dissociation, as well as improving molecular crystallization and orientation for efficient hole and electron transport in active layers. In this

[a]Key Laboratory of Luminescence and Optical Information, Ministry of Education, Beijing Jiaotong University, Beijing, 100044, China. E-mail: maxl@bjtu.edu.cn; fjzhang@bjtu.edu.cn

[b]Collaborative Innovation Center of Light Manipulations and Applications in Universities of Shandong, School of Physics and Electronics, Shandong Normal University, Jinan 250014, People's Republic of China. E-mail: qianqiansun@sdnu.edu.cn

[c]Department of Physics, Beijing Technology and Business University, Beijing, 100048, China

[d]Organic Optoelectronic Materials Laboratory, Department of Chemistry, College of Science, Korea University, Seoul, 02841, Republic of Korea

[e]Key Lab for Special Functional Materials, Ministry of Education, National and Local Joint Engineering Research Center for High-Efficiency Display and Lighting Technology, and School of Materials, Henan University, Kaifeng, 475004, Henan Province, China. E-mail: zzj@henu.edu.cn

† Electronic supplementary information (ESI) available. See https://doi.org/10.1039/d2ta02914f

Table 1 Key photovoltaic parameters of BHJ and LbL all-PSCs

Active layer	J_{SC} [mA cm^{-2}]	V_{OC} [V]	FF [%]	PCE [%]	Ref.
PBDB-T:N2200	11.89	0.867	64.4	6.58	16
PBDB-T/N2200	15.33	0.904	68.7	9.52	
PCE10:N2200	11.84	0.799	53.50	5.06	17
PCE10/N2200	12.30	0.796	53.96	5.26	
PBDB-T:PYT	22.64	0.887	70.02	14.06	
PBDB-T/PYT	23.03	0.891	73.98	15.17	
PBQx-H-TF:PBTIC-γ-TSe	23.17	0.91	65.85	13.91	18
PBQx-H-TF/PBTIC-γ-TSe	23.49	0.91	73.76	15.77	
PM6:PY-IT	22.29	0.95	72.24	15.29	This work
PM6/PY-IT	22.61	0.95	73.62	15.81	
PBDB-T/PYT	23.07	0.91	77	16.05	19
PM6:L15	22.51	0.95	71.31	15.19	20
PM6/L15	23.58	0.94	73.17	16.15	

work, an optimal PCE of 15.81% is achieved in LbL all-PSCs by adding CN to the acceptor solution.

Herein, a series of BHJ and LbL all-PSCs were composed of polymer PM6 as the donor, polymer PY-IT as the acceptor and CN as the solvent additive based on the normal structure of ITO/PEDOT:PSS/active layer/PNDIT-F3N/Al. The chemical structures, energy levels and absorption spectra of the used materials are exhibited in Fig. 1. The detailed HOMO and LUMO levels of the used materials are abstracted from ref. 21. The optimal LbL all-PSCs were achieved from PM6 chlorobenzene solution and PY-IT chloroform solution with 1 vol% CN, exhibiting a PCE of 15.81% along with an open circuit voltage (V_{OC}) of 0.95 V, a short circuit current density (J_{SC}) of 26.89 mA cm^{-2} and a fill factor (FF) of 75.79%. The optimal BHJ all-PSCs were achieved from the blend solutions with 1 vol% CN, exhibiting a PCE of 15.29% with an V_{OC} of 0.95 V, a J_{SC} of 22.29 mA cm^{-2} and an FF of 72.24%. The relatively large PCE (15.81% *vs.* 15.29%) of LbL all-PSCs *vs.* BHJ all-PSCs should benefit from the enhanced J_{SC} and FF due to the optimized photon harvesting, suppressed charge recombination and improved charge collection. This

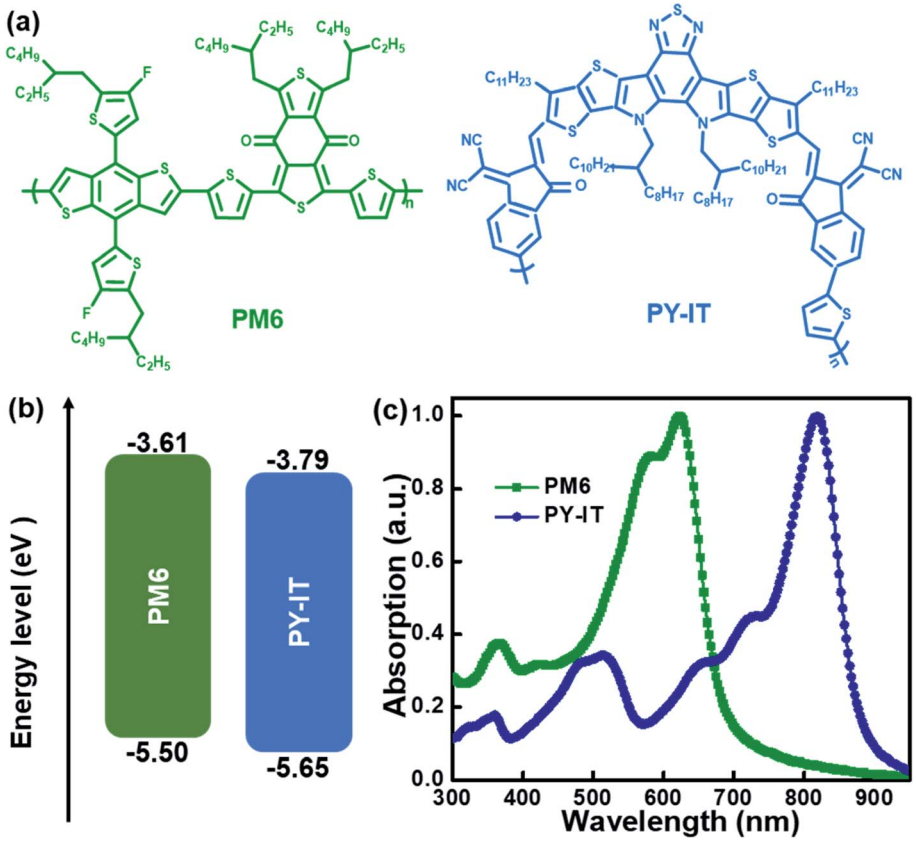

Fig. 1 (a) Chemical structures, (b) energy levels and (c) normalized absorption spectra of PM6 and PY-IT.

work suggests that using the LbL processing method combined with a solvent additive can optimize photo harvesting, charge transport and molecular arrangement to fabricate highly efficient all-PSCs.

Results and discussion

The current density *versus* applied voltage (*J*–*V*) curves of the BHJ and LbL all-PSCs were measured under AM 1.5 G illumination with 100 mW cm^{-2} light intensity, as displayed in Fig. 2a. The PCE of BHJ or LbL all-PSCs can be improved from 13.29% to 15.29% or from 13.67% to 15.81% by incorporating 1 vol% CN into the PM6:PY-IT blend solution or PY-IT solution, respectively. Over 15% PCE improvement can be obtained from BHJ and LbL all-PSCs with CN compared to the corresponding all-PSCs without CN. The performance improvement of all-PSCs is mainly attributed to J_{SC} enhancement from 20.76 mA cm^{-2} to 22.29 mA cm^{-2} for BHJ all-PSCs and from 21.12 mA cm^{-2} to 22.61 mA cm^{-2} for LbL all-PSCs, as well as FF increment from 67.36% to 72.24% for BHJ all-PSCs and from 68.14% to 73.62% for LbL all-PSCs. It should be noticed that the J_{SC} and FF of LbL all-PSCs are larger than those of the corresponding BHJ all-PSCs, which should be mainly due to the weakened charge recombination and more efficient charge transport channels in LbL active layers. The increased J_{SC} and FF of the BHJ and LbL all-PSCs with CN indicate that photon harvesting and morphology of active layers can be simultaneously improved by incorporating 1 vol% CN. The improved photon harvesting of BHJ and LbL all-PSCs with CN is well supported by the increased absorption spectra of the corresponding blend films incorporated with CN, as shown in Fig. S1.† To clarify the underlying reason for the effect of CN incorporation on the FF of all-PSCs, series resistance (R_S) and shunt resistance (R_{SH}) were calculated according to the *J*–*V* curves under light illumination. The R_{SH} and R_S are equal to differential resistance $\left(R = \frac{dV}{dJ}\right)$ when V_{OC} = 0 V and J_{SC} = 0 V. The BHJ or LbL all-PSCs with CN show a smaller R_S of 3.23 Ω cm^2 or 2.84 Ω cm^2 and a larger R_{SH} of 883 Ω cm^2 or 1031 Ω cm^2 than the corresponding all-PSCs without CN, which can well support the relatively large FF of all-PSCs with CN. It is commonly reported that efficient PSCs also exhibit relatively small R_S and relatively large R_{SH}.[22,23] The key photovoltaic parameters of all-PSCs and the calculated R_S as well as R_{SH} are summarized in Table 2.

The external quantum efficiency (EQE) spectra of all-PSCs were recorded and are exhibited in Fig. 2b. The calculated J_{SC}s

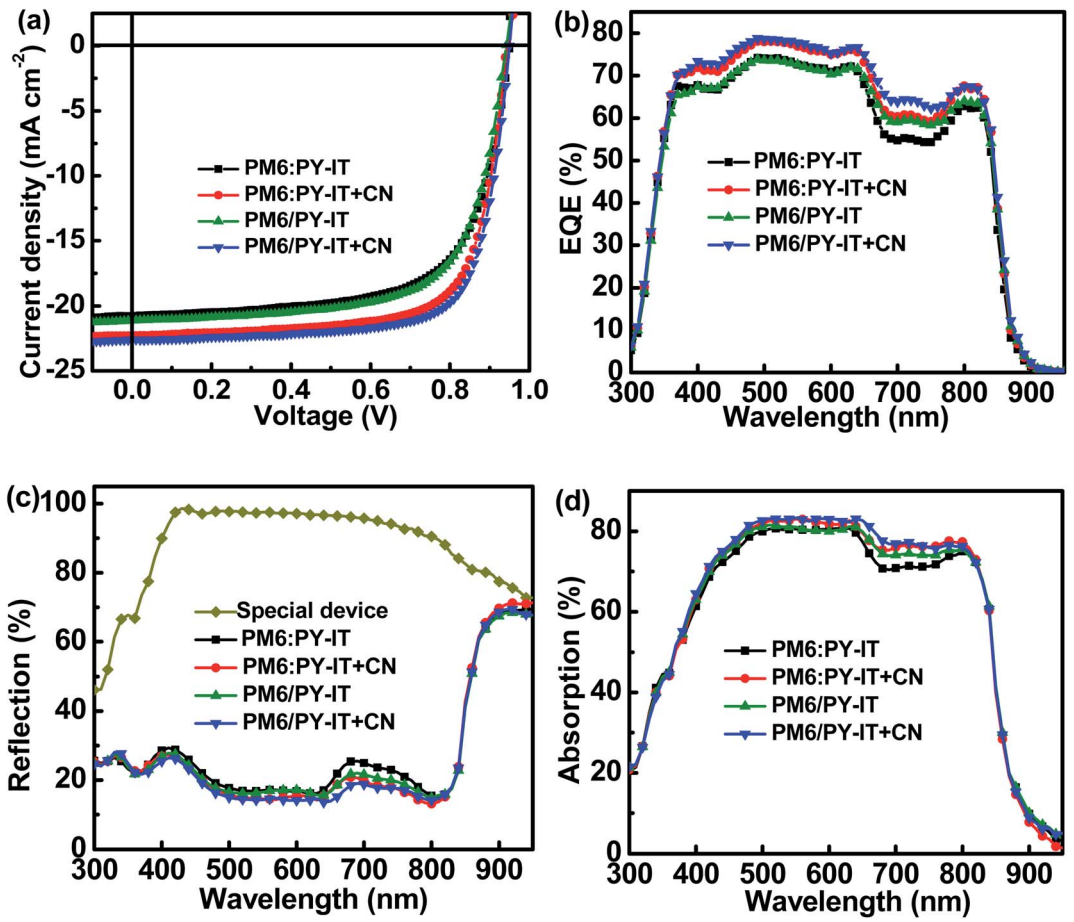

Fig. 2 (a) *J*–*V* curves of all-PSCs. (b) EQE spectra of all-PSCs. (c) Reflection spectra of all-PSCs and the special device. (d) Absorption spectra of active layers.

Table 2 Device parameters of the BHJ and LbL all-PSCs[a]

Active layer	J_{SC} [mA cm^{-2}]	Cal. J_{SC} [mA cm^{-2}]	V_{OC} [V]	FF [%]	PCE (ave. ± dev.) [%]	R_S [Ω cm^2]	R_{SH} [Ω cm^2]
PM6:PY-IT	20.76	19.78	0.95	67.36	13.29 (13.13 ± 0.16)	4.18	792
PM6:PY-IT + CN	22.29	21.21	0.95	72.24	15.29 (15.17 ± 0.12)	3.23	883
PM6/PY-IT	21.12	20.24	0.95	68.14	13.67 (13.52 ± 0.15)	3.77	806
PM6/PY-IT + CN	22.61	21.91	0.95	73.62	15.81 (15.69 ± 0.12)	2.84	1031

[a] The average and deviation (ave. ± dev.) of PCEs were calculated from 10 individual cells.

of all-PSCs with CN are higher than those of all-PSCs without CN, which agrees well with the tendency of the measured J_{SC}s. The detailed calculated J_{SC} values are listed in Table 2. The EQE values of all-PSCs with CN are larger than those of all-PSCs without CN in the wavelength range from 400 nm to 800 nm, which should be mainly caused by well-balanced photon harvesting, exciton dissociation, charge transport and collection in the corresponding all-PSCs with CN. To better understand the effect of employing CN on the EQE spectra of all-PSCs, the absorption spectra of the active layers in cells were investigated based on the reflection spectra of the relevant cells shown in Fig. 2c. A special cell ITO/PEDOT:PSS/poly(methyl methacrylate) PMMA/PNDIT-F3N/Al was constructed to investigate the influence of parasitic absorption in all-PSCs. The absorption spectra of the active layers in all-PSCs were evaluated using the difference between the reflection spectra of the specific device and those of all-PSCs, as exhibited in Fig. 2d.[24,25] The shape of the absorption spectra of the active layers is very similar to the shape of the corresponding EQE spectra. Increased EQE values in the spectral range from 650 nm to 750 nm can be observed for BHJ all-PSCs with the CN additive, which should be attributed to the improved exciton utilization efficiency obtained by incorporating the appropriate CN additive. Meanwhile, the EQE of LbL all-PSCs are larger than that of BHJ all-PSCs, suggesting that the molecular arrangement of PY-IT can be well adjusted in neat films by incorporating CN for harvesting more photons, as confirmed from Fig. 2b.

To unveil the charge generation and exciton dissociation properties in active layers, photogenerated current density (J_{ph}) *versus* effective voltage (V_{eff}) of all-PSCs were recorded, as displayed in Fig. 3a. Here, the J_{ph} is equal to the difference between the current density under AM 1.5G simulated solar illumination with 100 mW cm^{-2} light intensity (J_L) and that under dark conditions (J_D). The V_{eff} is defined as:

$$V_{eff} = V_{applied} - J \times R_s - V_0 \quad (1)$$

Here $V_{applied}$ and V_0 are the applied bias and the voltage under the $J_L = J_D$ condition, respectively.[22] The J_{ph} of all-PSCs can be defined as J_{ph}^{*}, $J_{ph}^{\&}$ and J_{sat} under the short-circuit, maximal output-power and saturated state conditions, respectively.[26–28] The J_{sat} values of both all-PSCs with the additive are higher than those of the corresponding all-PSCs without CN, indicating more efficient photon harvesting in the active layers with CN. The exciton dissociation efficiency (η_D) and charge collection efficiency (η_C) can be evaluated according to J_{ph}^{*}/J_{sat} and $J_{ph}^{\&}/J_{sat}$, respectively, as shown in Table S1†.[29–32] The η_D values of all-PSCs without or with CN are 92.92% or 94.61% for the BHJ structure, 92.66% or 94.43% for the LbL structure. The larger η_D for the BHJ all-PSCs should be mainly attributed to more PM6:PY-IT interfaces in the BHJ active layers. Benefiting from the more donor enrichment at the bottom of the LbL active layer and more acceptor enrichment at the top of the LbL active layer, the η_C values of LbL all-PSCs without or with CN are 81.51% or 82.11%, which are larger than the 80.92% or 82.01% of the corresponding BHJ all-PSCs.[33,34] It should be noticed that the η_D and η_C for all-PSCs with CN are higher than those of all-PSCs without CN, implying more effective exciton dissociation and charge collection in all-PSCs with CN. Furthermore, the photoluminescence (PL) spectra of pure PY-IT, PM6:PY-IT and PM6/PY-IT blend films without or with CN were investigated to further understand the exciton dissociation process in all-PSCs, as shown in Fig. 3b.[35,36] It is apparent that PY-IT has a strong and broad PL emission with a PL peak at 845 nm. The emission intensity of PY-IT is markedly quenched in the PM6:PY-IT and PM6/PY-IT blend films. Meanwhile, the PL emission intensity of the blend films with CN is lower than that of the corresponding blend films without CN, suggesting an increased exciton dissociation efficiency in the blend films with CN.

To better understand the impact of CN on the recombination dynamic process in the active layers, the *J*–*V* curves of all-PSCs were measured under different light intensities, as shown in Fig. S2.† Bimolecular recombination and space charge effects may result from the imbalanced hole and electron mobility, which are responsible for the dependence of J_{SC} values on P_{light} expressed as:

$$J_{SC} \propto P_{light}^{\ n} \quad (2)$$

as shown in Fig. 3c.[37–39] The fitted coefficient n represents the bimolecular recombination degree, and if the bimolecular recombination can be efficiently suppressed, it leads to an s value close to 1.[40,41] The n values of BHJ and LbL all-PSCs with CN are 0.962 and 0.969, which are larger than the 0.936 and 0.943 for all-PSCs without CN, respectively, indicating that bimolecular recombination can be restrained in all-PSCs by incorporating CN as the additive. The dependence of V_{OC} values on illumination P_{light} can be expressed as:

$$V_{OC} \propto s(KT/q)\ln P_{light} \quad (3)$$

In which K, T and q represent the Boltzmann constant, absolute temperature and elementary charge, respectively. The fitted coefficient s can give insight on the recombination process that

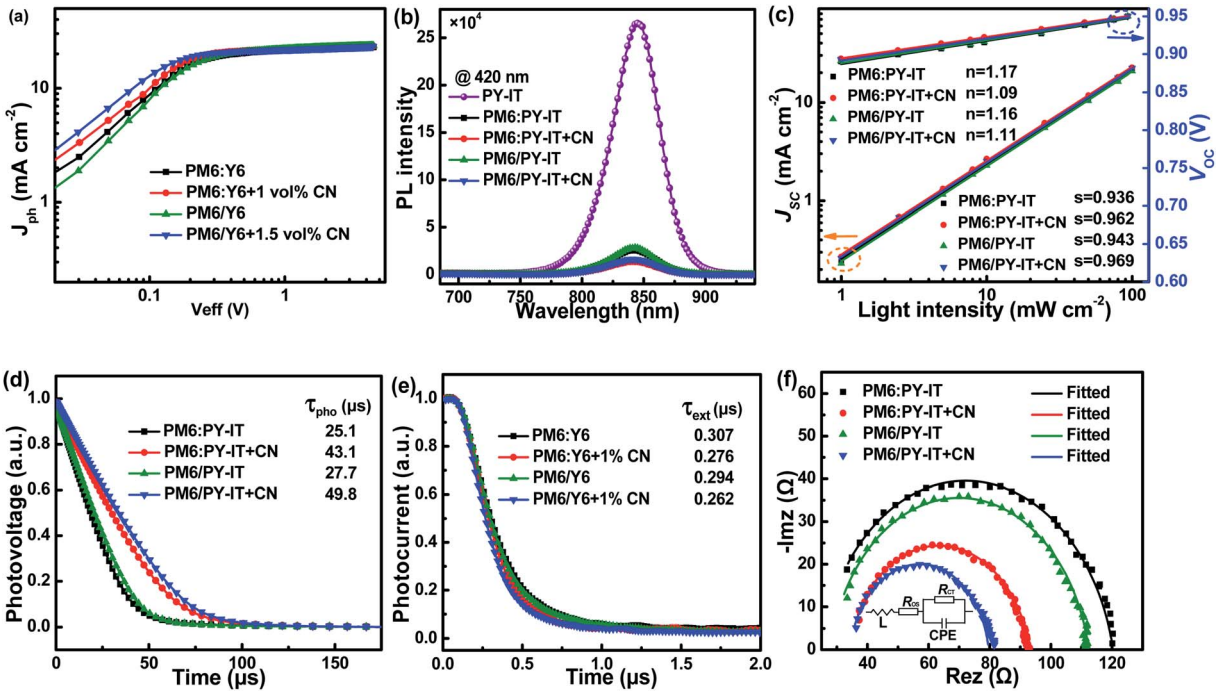

Fig. 3 (a) J_{ph}–V_{eff} curves of all-PSCs. (b) Photoluminescence spectra of the PY-IT film, and PM6:PY-IT and PM6/PY-IT blend films under 420 nm light excitation. (c) J_{sc}–P_{light} and V_{oc}–P_{light} curves of all-PSCs. (d) Transient photovoltage curves of all-PSCs. (e) Transient photocurrent curves of all-PSCs. (f) Nyquist plots and the equivalent circuit of all-PSCs.

dominates the devices. The *s* values of all-PSCs are larger than 1, which evidences the presence of Shockley–Read–Hall recombination in all-PSCs.[42,43] The charge recombination characteristic can be further explored from the transient photovoltage (TPV) measurement, as exhibited in Fig. 3d. The photocarrier lifetime (τ_{pho}) can be extracted from TPV curves under open-circuit conditions.[44–46] The τ_{pho} values of LbL or BHJ all-PSCs can be improved from 27.7 μs to 49.8 μs or from 25.1 μs to 43.1 μs by employing CN. The prolonged τ_{pho} values indicate restrained charge recombination in BHJ and LbL all-PSCs with CN. The charge extraction time (τ_{ext}) can be fitted from the transient photocurrent (TPC) decay curves under short-circuit conditions.[47–49] As shown in Fig. 3e, the fitted τ_{ext} values for BHJ and LbL all-PSCs with CN are 0.276 μs and 0.262 μs, which are

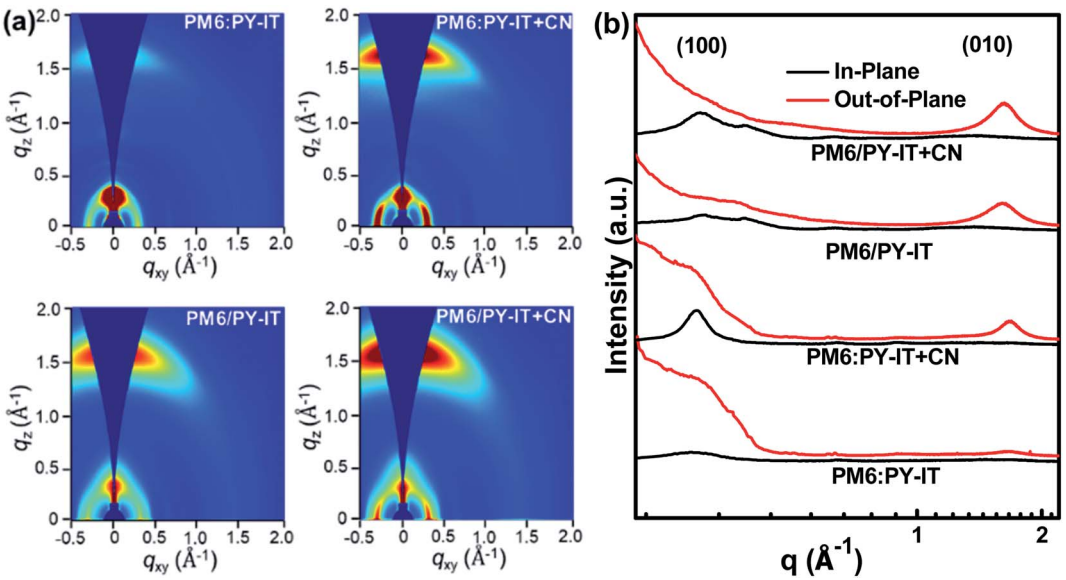

Fig. 4 (a) The 2D-GIWAXS patterns of PM6:PY-IT, PM6:PY-IT + CN, PM6/PY-IT and PM6/PY-IT + CN films. (b) The in-plane (IP, black line) and out-of-plane (OOP, red line) profiles abstracted from the 2D-GIWAXS patterns of the corresponding films.

shorter than the 0.307 μs and 0.294 μs for the BHJ and LbL all-PSCs without CN, respectively. The smaller τ_{ext} values reveal the efficient charge extraction in all-PSCs with CN. The longer photocarrier lifetime and the shorter charge extraction time can well support the enhanced JSC and FF in all-PSCs with CN.

To gain more insight into the charge transport and recombination process of all-PSCs, electrochemical impedance spectroscopy (EIS) measurements were carried out in the frequency range from 75 to 4.6 × 106 Hz under AM 1.5G illumination with 100 mW cm^{-2} light intensity. The Nyquist plots of all-PSCs measured at $V = V_{OC}$ are displayed in Fig. 3f and the inset shows the corresponding equivalent circuit model utilized to fit the Nyquist plot data. According to the equivalent circuit model, the fitting parameters of all-PSCs are listed in Table S2.† RCT represents charge transfer resistance, and ROS is associated with parasitic series resistance.[50–52] The all-PSCs with CN present smaller RCT and ROS, which are conducive to the more efficient charge transport in the active layers with CN. The constant phase element (CPE) is introduced to describe the non-ideal behavior of capacitors. The CPE is defined using CPET and CPEP values according to the equation:[53,54]

$$Z = (\mathrm{CPE_T})^{-1}(\mathrm{i}w)^{\mathrm{CPE_P}} \quad (4)$$

Z is the impedance of a CPE, w is the angular frequency, $\mathrm{CPE_T}$ is the capacitance value and $\mathrm{CPE_P}$ is the inhomogeneous constant varying between 0 and 1. The $\mathrm{CPE_P}$ values of BHJ or LbL all-PSCs are increased from 0.873 to 0.901 or from 0.886 to 0.912 by incorporating CN as the additive. The $\mathrm{CPE_P}$ values of BHJ and LbL all-PSCs with CN are much closer to 1 than those of the BHJ and LbL all-PSCs without CN, suggesting that there are fewer defects at the interface between PM6 and PY-IT as a result of employing CN. The time constant (τ) of the active layer associated with charge transfer can be calculated from the equation:[55]

$$\tau = R_{CT} \times \mathrm{CPE_T} \quad (5)$$

According to the R_{CT} and $\mathrm{CPE_T}$ values, the τ values are 761.52 ns and 771.69 ns for LbL all-PSCs with and without CN, and 906.30 ns and 964.44 ns for BHJ all-PSCs with and without CN, respectively. The relatively small τ values of all-PSCs with CN indicate inhibited charge recombination in the active layers with the CN additive.

Grazing incidence wide angle X-ray scattering (GIWAXS) characterization was employed to study the effect of introducing CN on molecular orientation properties. The 2D-GIWAXS patterns and the corresponding IP and OOP profiles of the neat films are exhibited in Fig. S3.† The neat PM6 film exhibits distinct (100) and (010) diffraction peaks in both OOP and IP directions, indicating the mixed face-on and edge-on molecular orientation of PM6. The intensity of the OOP (010) diffraction peak is enhanced in the PY-IT film with CN compared with that of the PY-IT film without CN, indicating that the face-on orientation of PY-IT is more ordered due to the incorporation of CN as the morphology regulator. The 2D-GIWAXS patterns and the corresponding OOP and IP profiles of the blend films are displayed in Fig. 4. The BHJ and LbL films exhibit the preferred face-on orientation, which is evidenced by the distinguishable lamellar stacking peak in the IP direction and the π–π stacking peak in the OOP direction. The positions of the diffraction peaks in the blend films are located between those of pure PM6 and PY-IT, signifying that the molecular arrangement in the blend films is codetermined by the donor and acceptor molecular arrangement.[56] Enhanced scattering intensity of the OOP (010) and IP (100) diffraction peaks can be observed from the profiles of the blend films with CN, indicating that a more ordered face-on molecular arrangement should be formed in the BHJ and LbL blend films with CN for efficient charge transport along the normal direction of the substrate.[57,58]

Conclusion

In summary, the LbL and BHJ all-PSCs were fabricated based on the wide bandgap polymer PM6 as the donor and the narrow bandgap polymer PY-IT as the acceptor. The LbL or BHJ all-PSCs with CN exhibit PCEs of 15.81% or 15.29% due to the incorporation of 1 vol% CN in PY-IT solution or PM6:PY-IT blend solution, resulting from the simultaneously improved J_{SC}s and FFs of LbL or BHJ all-PSCs with CN. Over 15% PCE improvement can be obtained in LbL or BHJ all-PSCs with CN, benefiting from the optimized photon harvesting, charge transport and molecular arrangement in LbL and BHJ active layers with CN. It should be highlighted that the PCEs of LbL all-PSCs are larger than those of the corresponding BHJ all-PSCs, which should be mainly due to the formation of more efficient charge transport channels by the LbL processing method. Overall, this work indicates that the LbL processing method combined with an additive should have great potential in preparing highly efficient all-PSCs.

Conflicts of interest

There are no conflicts of interest to declare.

Acknowledgements

This work was supported by the Fundamental Research Funds for the Central Universities (2022JBMC046) and the National Natural Science Foundation of China (62105017, 61975006, and 62175011).

References

1 J. Du, K. Hu, J. Zhang, L. Meng, J. Yue, I. Angunawela, H. Yan, S. Qin, X. Kong, Z. Zhang, B. Guan, H. Ade and Y. Li, *Nat. Commun.*, 2021, **12**, 5264.
2 J. Zhang, C. Tan, K. Zhang, T. Jia, Y. Cui, W. Deng, X. Liao, H. Wu, Q. Xu, F. Huang and Y. Cao, *Adv. Energy Mater.*, 2021, **11**, 2102559.
3 Z. Genene, J. Lee, S. Lee, Q. Chen, Z. Tan, B. Abdulahi, D. Yu, T. Kim, B. Kim and E. Wang, *Adv. Mater.*, 2022, **34**, 2107361.
4 H. Fu, Y. Li, J. Yu, Z. Wu, Q. Fan, F. Lin, H. Woo, F. Gao, Z. Zhu and A. Jen, *J. Am. Chem. Soc.*, 2021, **143**, 2665–2670.

5 Y. Zhang, B. Wu, Y. He, W. Deng, J. Li, J. Li, N. Qiao, Y. Xing, X. Yuan, N. Li, C. Brabec, H. Wu, G. Lu, C. Duan, F. Huang and Y. Cao, *Nano Energy*, 2022, **93**, 106858.
6 F. Cui, Z. Chen, J. Qiao, T. Wang, G. Lu, H. Yin and X. Hao, *Adv. Funct. Mater.*, 2022, **32**, 2200478.
7 R. Sun, Y. Wu, X. Yang, Y. Gao, Z. Chen, K. Li, J. Qiao, T. Wang, J. Guo, C. Liu, X. Hao, H. Zhu and J. Min, *Adv. Mater.*, 2022, **34**, 2110147.
8 C. He, Y. Pan, Y. Ouyang, Q. Shen, Y. Gao, K. Yan, J. Fang, Y. Chen, C. Ma, J. Min, C. Zhang, L. Zuo and H. Chen, *Energy Environ. Sci.*, 2022, DOI: **10.1039/d2ee00595f**.
9 X. Xu, L. Yu, H. Meng, L. Dai, H. Yan, R. Li and Q. Peng, *Adv. Funct. Mater.*, 2021, **31**, 2108797.
10 Y. Zheng, R. Sun, M. Zhang, Z. Chen, Z. Peng, Q. Wu, X. Yuan, Y. Yu, T. Wang, Y. Wu, X. Hao, G. Lu, H. Ade and J. Min, *Adv. Energy Mater.*, 2021, **11**, 2102135.
11 D. Li, C. Guo, X. Zhang, B. Du, C. Yu, P. Wang, S. Cheng, L. Wang, J. Cai, H. Wang, D. Liu, H. Yao, Y. Sun, J. Hou and T. Wang, *Sci. China: Chem.*, 2022, **65**, 373–381.
12 Y. Cui, S. Zhang, N. Liang, J. Kong, C. Yang, H. Yao, L. Ma and J. Hou, *Adv. Mater.*, 2018, **30**, 1802499.
13 X. Wang, L. Zhang, L. Hu, Z. Xie, H. Mao, L. Tan, Y. Zhang and Y. Chen, *Adv. Funct. Mater.*, 2021, **31**, 2102291.
14 Q. Li, L. Wang, S. Liu, L. Guo, S. Dong, G. Ma, Z. Cao, X. Zhan, X. Gu, T. Zhu, Y. Cai and F. Huang, *ACS Energy Lett.*, 2020, **5**, 3637–3646.
15 W. Xu, X. Li, S. Jeong, J. Son, Z. Zhou, Q. Jiang, H. Woo, Q. Wu, X. Zhu, X. Ma and F. Zhang, *J. Mater. Chem. C*, 2022, **10**, 5489–5496.
16 Y. Xu, J. Yuan, S. Liang, J. Chen, Y. Xia, B. Larson, Y. Wang, G. Su, Y. Zhang, C. Cui, M. Wang, H. Zhao and W. Ma, *ACS Energy Lett.*, 2019, **4**, 2277–2286.
17 Q. Wu, W. Wang, Y. Wu, Z. Chen, J. Guo, R. Sun, J. Guo, Y. Yang and J. Min, *Adv. Funct. Mater.*, 2021, **31**, 2010411.
18 C. Cao, H. Wang, D. Qiu, T. Zhao, Y. Zhu, X. Lai, M. Pu, Y. Li, H. Li, H. Chen and F. He, *Adv. Funct. Mater.*, 2022, **32**, 2201828.
19 Y. Zhang, B. Wu, Y. He, W. Deng, J. Li, J. Li, N. Qiao, Y. Xing, X. Yuan, N. Li, C. Brabec, H. Wu, G. Lu, C. Duan, F. Huang and Y. Cao, *Nano Energy*, 2022, **93**, 106858.
20 B. Li, X. Zhang, Z. Wu, J. Yang, B. Liu, Q. Liao, J. Wang, K. Feng, R. Chen, H. Woo, F. Ye, L. Niu, X. Guo and H. Sun, *Sci. China: Chem.*, 2022, **65**, 1157–1163.
21 T. Liu, T. Yang, R. Ma, L. Zhan, Z. Luo, G. Zhang, Y. Li, K. Gao, Y. Xiao, J. Yu, X. Zou, H. Sun, M. Zhang, T. Dela Peña, Z. Xing, H. Liu, X. Li, G. Li, J. Huang, C. Duan, K. Wong, X. Lu, X. Guo, F. Gao, H. Chen, F. Huang, Y. Li, Y. Li, Y. Cao, B. Tang and H. Yan, *Joule*, 2021, **5**, 914–930.
22 J. Vollbrecht, V. Brus, S. Ko, J. Lee, A. Karki, D. Cao, K. Cho, G. Bazan and T. Nguyen, *Adv. Energy Mater.*, 2019, **9**, 1901438.
23 J. Vollbrecht and V. Brus, *Org. Electron.*, 2020, **86**, 105905.
24 X. Ma, A. Zeng, J. Gao, Z. Hu, C. Xu, J. Son, S. Jeong, C. Zhang, M. Li, K. Wang, H. Yan, Z. Ma, Y. Wang, H. Woo and F. Zhang, *Natl. Sci. Rev.*, 2021, **8**, nwaa305.
25 X. Wang, Q. Sun, J. Gao, J. Wang, C. Xu, X. Ma and F. Zhang, *Energies*, 2021, **14**, 4200.
26 M. Nam, J. Na, J. Shin, H. Lee, R. Chang and D. Ko, *Nano Energy*, 2020, **74**, 104883.
27 K. Yang, J. Wang, Z. Zhao, Y. Sun, M. Liu, Z. Zhou, X. Zhang and F. Zhang, *Chem. Eng. J.*, 2022, **435**, 134973.
28 M. Jiang, H. Bai, H. Zhi, J. Sun, J. Wang, F. Zhang and Q. An, *ACS Energy Lett.*, 2021, **6**, 2898–2906.
29 C. Yan, H. Tang, R. Ma, M. Zhang, T. Liu, J. Lv, J. Huang, Y. Yang, T. Xu, Z. Kan, H. Yan, F. Liu, S. Lu and G. Li, *Adv. Sci.*, 2020, **7**, 2000149.
30 S. Zhang, X. Ma, C. Xu, W. Xu, S. Jeong, H. Woo, Z. Zhou, X. Zhang and F. Zhang, *Macromol. Rapid Commun.*, 2022, **43**, 2200345.
31 X. Ma, Q. An, O. Ibraikulov, P. Lévêque, T. Heiser, N. Leclerc, X. Zhang and F. Zhang, *J. Mater. Chem. A*, 2020, **8**, 1265–1272.
32 R. Yu, G. Wu, Y. Cui, X. Wei, L. Hong, T. Zhang, C. Zou, S. Hu, J. Hou and Z. Tan, *Small*, 2021, **17**, 2103497.
33 W. Xu, X. Ma, J. Son, S. Jeong, L. Niu, C. Xu, S. Zhang, Z. Zhou, J. Gao, H. Woo, J. Zhang, J. Wang and F. Zhang, *Small*, 2022, **18**, 2104215.
34 M. Liu, J. Wang, K. Yang, Z. Zhao, Z. Zhou, Y. Ma, L. Shen, X. Ma and F. Zhang, *J. Mater. Chem. C*, 2021, **9**, 6357–6364.
35 H. Ning, Q. Jiang, P. Han, M. Lin, G. Zhang, J. Chen, H. Chen, S. Zeng, J. Gao, J. Liu, F. He and Q. Wu, *Energy Environ. Sci.*, 2021, **14**, 5919–5928.
36 Z. Zhao, B. Liu, C. Xie, Y. Ma, J. Wang, M. Liu, K. Yang, Y. Xu, J. Zhang, W. Li, L. Shen and F. Zhang, *Sci. China: Chem.*, 2021, **64**, 1302–1309.
37 P. Heremans, L. Koster, M. Muccini, V. Mihailetchi, R. Ramaker, E. Meulenkamp, H. Xie and P. Blom, *Appl. Phys. Lett.*, 2006, **86**, 123509.
38 L. Koster, V. Mihailetchi, H. Xie and P. W. Blom, *Appl. Phys. Lett.*, 2005, **87**, 203502.
39 J. Vollbrecht, J. Lee, S. Ko, V. Brus, A. Karki, W. Le, M. Seifrid, M. Ford, K. Cho, G. Bazan and T. Nguyen, *J. Mater. Chem. C*, 2020, **8**, 15175–15182.
40 H. Chen, T. Zhao, L. Li, P. Tan, H. Lai, Y. Zhu, X. Lai, L. Han, N. Zheng, L. Guo and F. He, *Adv. Mater.*, 2021, **33**, 2102778.
41 C. Xu, Z. Zhao, K. Yang, L. Niu, X. Ma, Z. Zhou, X. Zhang and F. Zhang, *J. Mater. Chem. A*, 2022, **10**, 6291–6329.
42 V. Brus, *Org. Electron.*, 2016, **29**, 1–6.
43 V. Brus, C. Proctor, N. Ran and T. Nguyen, *Adv. Energy Mater.*, 2016, **6**, 1502250.
44 A. Chatri, S. Torabi, V. Corre and L. Koster, *ACS Appl. Mater. Interfaces*, 2018, **10**, 12013–12020.
45 Y. Lin, Y. Firdaus, F. Isikgor, M. Nugraha, E. Yengel, G. Harrison, R. Hallani, A. Labban, H. Faber, C. Ma, X. Zheng, A. Subbiah, C. Howells, O. Bakr, I. Culloch, S. Wolf, L. Tsetseris and T. Anthopoulos, *ACS Energy Lett.*, 2020, **5**, 2935–2944.
46 Z. Zhao, M. Liu, K. Yang, C. Xu, Y. Guan, X. Ma, J. Wang and F. Zhang, *Adv. Funct. Mater.*, 2021, **31**, 2106009.
47 V. Corre, A. Chatri, N. Doumon and L. Koster, *Adv. Energy Mater.*, 2017, **7**, 1701138.
48 R. Wang, D. Zhang, S. Xie, J. Wang, Z. Zheng, D. Wei, X. Sun, H. Zhou and Y. Zhang, *Nano Energy*, 2018, **51**, 736–744.
49 W. Gao, T. Liu, R. Sun, G. Zhang, Y. Xiao, R. Ma, C. Zhong, X. Lu, J. Min, H. Yan and C. Yang, *Adv. Sci.*, 2020, **7**, 1902657.

50 Z. Zhao, C. Xu, Y. Ma, K. Yang, M. Liu, X. Zhu, Z. Zhou, L. Shen, G. Yuan and F. Zhang, *Adv. Funct. Mater.*, 2022, **32**, 2203606.
51 X. Ma, C. Tang, Y. Ma, X. Zhu, J. Wang, J. Gao, C. Xu, Y. Wang, J. Zhang, Q. Zheng and F. Zhang, *ACS Appl. Mater. Interfaces*, 2021, **13**, 57684–57692.
52 T. Kumari, S. Lee, K. Lee, Y. Cho and C. Yang, *Adv. Energy Mater.*, 2018, **8**, 1800616.
53 W. Li, J. Cai, F. Cai, Y. Yan, H. Yi, R. Gurney, D. Liu, A. Iraqi and T. Wang, *Nano Energy*, 2018, **44**, 155–163.
54 C. Xu, X. Ma, Z. Zhao, M. Jiang, Z. Hu, J. Gao, Z. Deng, Z. Zhou, Q. An, J. Zhang and F. Zhang, *Sol. RRL*, 2021, **5**, 2100175.
55 B. Xiao, M. Zhang, J. Yan, G. Luo, K. Gao, J. Liu, Q. You, H. Wang, C. Gao, B. Zhao, X. Zhao, H. Wu and F. Liu, *Nano Energy*, 2017, **39**, 478–488.
56 K. Yang, Z. Zhao, M. Liu, Z. Zhou, K. Wang, X. Ma, J. Wang, Z. He and F. Zhang, *Chem. Eng. J.*, 2022, **427**, 131802.
57 K. Jiang, J. Zhang, Z. Peng, F. Lin, S. Wu, Z. Li, Y. Chen, H. Yan, H. Ade, Z. Zhu and A. Jen, *Nat. Commun.*, 2021, **12**, 468.
58 C. Xu, K. Jin, Z. Xiao, Z. Zhao, Y. Yan, X. Zhu, X. Li, Z. Zhou, S. Jeong, L. Ding, H. Woo, G. Yuan and F. Zhang, *Sol. RRL*, 2022, **6**, 2200308.